

Positioning of Longitudinal Nerves in *C. elegans* by Nidogen

Seonhee Kim and William G. Wadsworth*

Basement membranes can help determine pathways of migrating axons. Although members of the nidogen (entactin) protein family are structural components of basement membranes, we find that nidogen is not required for basement membrane assembly in the nematode *Caenorhabditis elegans*. Nidogen is localized to body wall basement membranes and is required to direct longitudinal nerves dorsoventrally and to direct axons at the midlines. By examining migration of a single axon *in vivo*, we show that nidogen is required for the axon to switch from circumferential to longitudinal migration. Specialized basement membranes may thus regulate nerve position.

The nervous system is organized into longitudinal and circumferential projections. As the axon scaffold forms, migrating growth cones can switch between circumferential and longitudinal directions. Members of several protein families, including netrin, semaphorin, ephrin, and slit, act as attractive or repulsive guidance molecules to direct axons to their targets (1). Changes in the responsiveness of migrating axons to such guidance molecules could in part underlie the ability of axons to migrate in new directions. Also important for determining where pioneering axons migrate are the physical substrates that support the nervous system, including the basement membranes.

In order to identify genes required for the placement of nerves, we selected mutations that affect the position of nerves, but do not affect axon outgrowth. From a clonal F₂ screen of approximately 6000 haploid genomes treated with the mutagen ethylmethanesulfonate, we identified 11 mutations that define several loci (2). We chose one allele, *ur41*, that disrupts the *nid-1* locus and is a loss-of-function allele, causing nerves to form at the wrong positions. Most neural circuits in animals with this mutation are apparently formed normally, as the animals show wild-type behavior instead of the uncoordinated (Unc) phenotype. In general, morphogenesis is normal, and the animals do not have traits that are sometimes associated with cell migration defects. For example, they do not have a dumpy (Dpy) appearance, they are not egg-laying defective (Egl), nor do they have misformed gonads.

In more than 90% of the *nid-1(ur41)* mutants, the dorsal sublateral nerves are mispositioned to the dorsal midline (Fig. 1, A and B, and Table 1A). Although mispositioned, the axons appear normal, and they form normal bundles (Fig. 2B). We also observe that in 32% of the mutants ($n = 100$) the ventral nerve axons overpopulate the left fascicle of the ven-

tral nerve cord and underpopulate the right fascicle (Fig. 1, C and D). Thus, instead of the normal asymmetric phenotype of the *C. elegans* ventral nerve cord, the cord is nearly symmetric (Fig. 2A). We examined the phenotypes of *nid-1(ur41)* animals in greater detail (3). Besides defects in controlling the position of specific nerves, we did not observe other defects by electron microscopy. The tissues and basement membranes that support the nervous system are essentially normal (Fig. 2C). Moreover, axons that are not affected by the *nid-1(ur41)* mutation cross without difficulty the same surfaces that affected axons cross. These observations suggest that the altered positions of nerves are not a secondary consequence of an extensively disrupted substratum.

We observed individual classes of ventral neurons marked with green fluorescent protein (GFP) reporters in the *nid-1(ur41)* mutant. In wild-type animals, ventral nerve cord interneurons contribute to the normal asymmetry of the cord, as can be seen in a bundle of interneuron axons that exits the nerve ring from the left side and then crosses over to the right fascicle (Fig. 1, E and F, and Table 1C). In *nid-1(ur41)*, the right tract is correctly established, but the crossing of the axon bundle from the left to right side is impaired. The axons still cross but not in the appropriate place, and they cross in small bundles or as individual axons. The PVQ axons were also examined because they help to initiate the extension of the ventral nerve cord from posterior ganglia (4). In *nid-1(ur41)*, the left PVQ axon often fails to initiate the left tract and instead crosses the midline and travels with the right PVQ axon in the right fascicle (Fig. 1, G and H, and Table 1B). The migration of the right PVQ axon is not affected. We also examined the postembryonic HSN neurons, because HSN axon migration to the ventral nerve cord may require PVQ axons (5). We find that, like the PVQ axons, HSNL, but not HSNR, axon migrations are defective in *nid-1(ur41)* (6). These phenotypes suggest that there is a defect associated with axons approaching the ventral midline from the left side.

In the *nid-1(ur41)* mutant, longitudinal mo-

tor neuron axons that should be in the right fascicle are instead in the left. The motor neurons are arranged in a line at the ventral midline with the two fascicles of the ventral nerve cord flanking the cell bodies (Fig. 1C). Some motor neurons have two processes that grow out in different directions. In wild-type animals, one process joins the right fascicle; the other extends circumferentially to the dorsal midline. In the *nid-1* mutant, the circumferential processes are normal, but the longitudinal processes frequently join the left fascicle (Fig. 1, I and J, and Table 1D). This abnormality accounts for the overpopulated left fascicle of the ventral cord, and it suggests that these axons initially fail to distinguish between the left and right sides of the ventral midline. Once the axons adopt a side, however, they apparently respect the midline, for they do not repeatedly cross the midline, and the two fascicles remain apart.

In *nid-1(ur41)*, the dorsal nerve cord has a split appearance. In wild-type animals, the dorsal nerve cord is formed by axons from the ventral midline motor neurons that migrate to the dorsal midline, bifurcate, and extend processes longitudinally along the left side of the midline. Motor neuron axons that migrate circumferentially along the right body wall cross the dorsal midline to join the nerve. In *nid-1(ur41)* mutants, these motor neuron axons bifurcate and migrate longitudinally on the right side of the midline before crossing (Fig. 1, K and L, and Table 1E). Those that reach the tract from the left side appear normal. These results suggest that axons from the right side are not effectively guided across the midline.

Because the axon migration phenotypes at the midline show left versus right differences, we examined other features of the animal that are asymmetric, and we conclude that the left and right differences in *nid-1(ur41)* are confined to the axons at the midline. For example, the stereotyped side that each motor neuron axon and distal tip cell circumferentially migrates across is preserved in *nid-1(ur41)*. Also, the anterior migration of the right Q cell and posterior migration of the left Q cell are normal. These results indicate that *nid-1* does not affect the overall handedness of the animal.

To identify the protein product of *ur41*, we mapped the mutation to a region that is one-half map unit in size (Fig. 3A). Using cosmids that corresponded to the region, we cloned the *ur41* locus by DNA-mediated transformation rescue of the *ur41* dorsal sublateral nerve and ventral nerve cord phenotypes. One cosmid, F54F3, was capable of rescuing the phenotypes. DNA sequence analysis predicts that this cosmid contains the gene that encodes the single *C. elegans* homolog of nidogen (entactin) (*C. elegans* Genome Sequencing Consortium, Fig. 3B). We found that a genomic fragment, enhanced by the polymerase chain reaction (PCR), that contains the predicted nidogen (entactin) coding sequences and 2.5 kb of 5' flanking sequence

Department of Pathology, Robert Wood Johnson Medical School, Piscataway, NJ 08854-5635, USA.

*To whom correspondence should be addressed. E-mail: wadsworth@umdnj.edu

REPORTS

can rescue the *ur41* phenotypes. Furthermore, animals with the same phenotype as *ur41* mutants are observed when loss of *nid-1* function is phenocopied by RNA-mediated interference (7). DNA sequence analysis of *ur41* identifies a nonsense point mutation introducing a stop in the first third of the predicted protein (8) (Fig. 3B). This is consistent with having the allele behave genetically as a null, that is, the mutant phenotypes are not more severe in animals with *ur41* in *trans* to a genetic deficiency that eliminates the *nid-1* locus than in *ur41* homozygous animals.

Nidogen (entactin) is a basement membrane component that is highly conserved among human, *Drosophila*, *C. elegans*, and ascidians (9). The protein comprises three globular domains (G1, G2, and G3) connected by a flexible linker and a rod-like domain that includes epidermal growth factor (EGF)-like modules (10, 11). It is proposed that nidogen-1 connects laminin and collagen IV networks together to form stable basement membranes (9–11). Vertebrate nidogen promotes cell migrations *in vitro*, and antibodies that block the laminin-nidogen interaction disrupt tissue morphogenesis (12–15). Al-

though models predict that nidogen is a structural component of basement membranes, basement membranes assemble normally, and in general, tissues and their basement membranes appear to develop normally in the *C. elegans* nidogen mutant.

Larvae stained with anti-nidogen antiserum show that nidogen is localized to body wall basement membranes (16). Intense staining is associated with the basement membrane of the body wall muscle (Fig. 4, A and B). Staining is not detected in *nid-1(ur41)* animals [Web fig. 1 (17)]. Nidogen can bind collagen type IV, fibulins, laminin, and perlecan (10, 18, 19). It is interesting that both collagen type IV and perlecan in *C. elegans* are selectively distributed to the basement membranes between the epidermis and body wall muscles (20, 21). Each sublateral nerve runs longitudinally along the center margin of a muscle quadrant, sandwiched between the basement membrane and the epidermis; nerve cords run longitudinally along the edges of the interface between muscle and basement membranes and epidermis. Possibly nidogen is incorporated differently into this membrane and has distinct regulatory func-

tions at these sites. This would be consistent with a model that multiple guidance cues, distributed in gradients and associated with the different tissues, and specialized basement membranes, form unique combinations at each dorsoventral position to specify where the different longitudinal nerves form (22, 23).

To examine the expression pattern of *nid-1*, we used *in situ* hybridization analysis and GFP expression under the control of the *nid-1* promoter sequence (24). Expression of the GFP transcription reporter is first detected in late gastrulation by the cephalic, inner labial, and outer labial cells (Fig. 5). As the embryo elongates and morphogenesis begins, expression in body wall muscle cells is detected by *in situ* hybridization [Web fig. 2 (17)] and is observed by using the GFP reporter. In addition, GFP is observed in the left and right lateral ALM neurons and the anal depressor and intestinal muscle cells. As embryogenesis continues, expression in the body wall muscle declines and is not observed in the larval stages. During the larval and adult stages, GFP expression by the PLM neurons, the intestinal cells, and the distal tip cells of the gonad is observed. In addition, transient expression is observed in HSN neurons during the L3 and L4 stages and in ventral nerve cord neurons during the early L2 stage. Although these observations are limited by the sensitivity of *in situ* hybridization and the ability of the *nid-1* promoter sequence to reproduce the wild-type *nid-1* expression pattern, they suggest that the *nid-1* gene is not expressed by the axons affected in the *nid-1(ur41)* mutant.

Because *nid-1* encodes a secreted matrix protein and is required to position axons, we asked whether it might have activities similar to those of known extracellular guidance molecules. We expressed *nid-1* in neurons, intestinal cells, and body wall muscles to determine how ectopic expression affects nerve development

Fig. 1. Effects of *nid-1* on positioning longitudinal nerves and axons. (A, C, E, G, I, and K) Wild-type *C. elegans* nematodes; (B, D, F, H, J, and L) *nid-1(ur41)* mutant nematodes. (A and B) The dorsal sublateral nerve (*dsl*) becomes mispositioned along the dorsal nerve cord (*dc*) in the mutant. Neurons are identified by GFP fluorescence to show expression of an *unc-119::GFP* transgene as a pan-neural marker. Lateral aspect. (C and D) Compared with the wild type, in the mutant there are more ventral nerve cord axons in the left fascicle (small arrowhead) and fewer in the right (large arrowhead). Neurons are visualized by pan-neural *unc-119::GFP* expression. Ventral aspect. (E and F) Interneuron axons that exit from the head on the left crossover (arrow) to the right fascicle (large arrowhead) at the anterior end of the ventral nerve cord. In the mutant, the axons cross at multiple positions (arrows) and sometime remain in the left fascicle for some distance (small arrowhead). Neurons are identified by expression of *glr-1::GFP*, a marker for interneurons of the right fascicle. Ventral aspect. (G and H) In the wild type, the PVQR axon is in the right fascicle (large arrowhead) and PVQL is in the left fascicle (small arrowhead). In the mutant, PVQL crosses to the right fascicle. These axons flank the vulva (*v*). Neurons are identified by expression of *sra-6::GFP*, a marker for PVQ in the posterior ventral nerve cord. Ventral aspect. (I and J) In the wild type, the longitudinal processes of the motor neurons are in the right fascicle (large arrowhead); whereas in the mutant, the processes also populate the left fascicle (small arrowhead). Circumferential processes are normal. Neurons are identified by expression of a *unc-129::GFP* transgene, a marker for DA and DB motor neurons. Ventral aspect. (K and L) To form the dorsal nerve cord (large arrowhead), axons from the ventral motor neurons migrate along both sides of the body to the dorsal midline. The cord forms along the left side of the midline. In the mutant, axons that migrate dorsally on the right side bifurcate and migrate along the right side of the midline (small arrowhead) before crossing over. Neurons are identified by expression of the *unc-129::GFP* transgene. Dorsal aspect. Anterior is to the left in all micrographs.

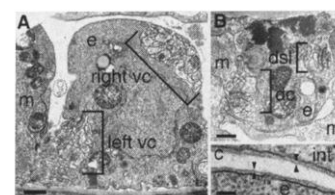
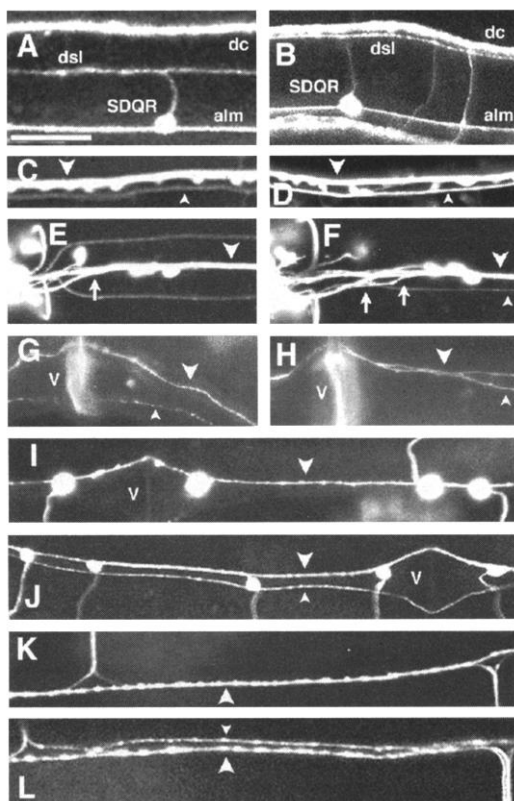


Fig. 2. Electron micrographs of *nid-1(ur41)* larva. (A) Cross section through the ventral epidermal ridge. In the wild type, there are approximately 54 axons in the right fascicle and 6 in the left fascicle (28), in the mutant there are, on average, 25 ± 2 axons in the left and 29 ± 3 in the right ($n = 3$). Scale bar, 500 nm. (B) Cross section through the dorsal epidermal ridge. The dorsal nerve cord (*dc*) is positioned along the left side of the epidermal (*e*) ridge. A mispositioned dorsal sublateral nerves (*dsl*) is positioned along the right side of the ridge. Axon morphology is normal. Scale bar, 500 nm. (C) As in the wild-type animals, intact basement membranes (between arrow heads) assemble at tissues, including the intestine (*int*) and epidermis (*e*). Scale bar, 100 nm.

(24). Staining of these strains with the anti-nidogen antiserum shows wild-type protein distribution (25), suggesting that the incorporation of nidogen is specific to the local assembly of the body wall basement membranes. We find that ectopic expression from any source rescues the *nid-1* mutant phenotypes, causing the nerves to be correctly positioned. In contrast, ectopic expression of netrin UNC-6 or transforming growth factor- β UNC-129 causes anomalous axon migrations that are consistent

with the idea that the distributions of attractant and repellent guidance molecules are altered by the ectopic expression (22, 23, 26). Together these observations indicate that nidogen and chemotropic guidance factors function differently to position nerves.

We used the migration of the SDQR axon to study the positioning of dorsal sublateral axons. In the first larval stage, the SDQR axon is repelled dorsally from ventral netrin UNC-6 sources until it reaches the dorsal sublateral

position. There, the responsiveness to UNC-6 changes, and the axon migrates anteriorly (22). In *unc-6* mutants, SDQR migrates ventrally, presumably in response to some other cues that are unmasked by the absence of UNC-6. We now find that *nid-1* is also required to position SDQR dorsoventrally. However, although *unc-6* is required for the SDQR axon to be directed dorsally, *nid-1* is necessary to prevent the axon from migrating past the dorsal sublateral position to the dorsal midline. In 54% of the *nid-1(ur41)* mutants ($n = 100$), the SDQR axon migrates to the dorsal midline (Table 2). This phenotype is never observed in *unc-6* mutants or when *unc-6* is ectopically expressed (22, 23). We also note that the SDQR axon, as well as other circumferentially migrating axons, migrate directly across the dorsal sublateral basement membrane in the *nid-1(ur41)* mutant, indicating that the lack of nidogen has not affected the ability of axons to migrate across this surface.

Because the netrin receptor genes, *unc-5* and *unc-40*, also affect SDQR migrations, we examined the relationship between *nid-1* and these genes. In *unc-5*, *unc-6*, or *unc-40* mutants, the SDQR axon never migrates past the dorsal sublateral position to the dorsal midline [$n = 100$ for each; see also (22)]. However, in a few *unc-5; nid-1* and *nid-1; unc-6* double mutants where the SDQR axon does reach the dorsal region, the axon will migrate to the dorsal midline (for *unc-5; nid-1* mutants, 5% turn at the dorsal sublateral tract and 3% migrate to the dorsal midline and for *nid-1; unc-6* mutants, 5% turn at the dorsal sublateral tract and 2% migrate to the dorsal midline; $n = 100$ for each). In contrast, the SDQR axon never migrates to the dorsal midline in *unc-40; nid-1* mutants (Table 2), but instead is guided anteriorly at the dorsal sublateral position (65%, $n = 100$). This migration again indicates that this basement membrane, even when lacking nidogen, can support axon migrations. Furthermore, this shows that *unc-40* is epistatic to *nid-1*, that is, the double mutants display the *unc-40* phenotype instead of the *nid-1* phenotype, indicating that these genes function together to direct the circumferential to longitudinal turn of the

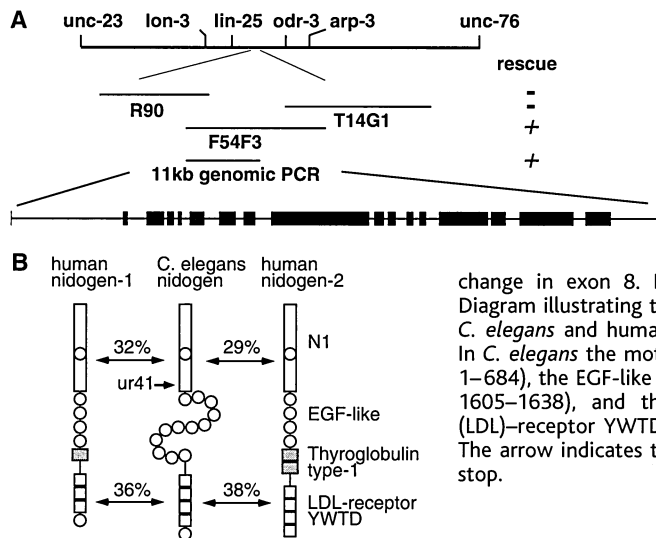


Fig. 3. The *nid-1* gene and protein. **(A)** Molecular cloning. The *nid-1* gene maps between *lin-25* and *odr-3* of linkage group V. The cosmid F54F3 rescues *nid-1(ur41)* as does an 11-kb PCR fragment. The *ur41* mutation introduces a CAA→TAA change in exon 8. Black boxes are exons. **(B)** Diagram illustrating the domain structures of the *C. elegans* and human nidogen family members. In *C. elegans* the motifs are the N1 (amino acids 1–684), the EGF-like (amino acids 685–1320 and 1605–1638), and the low density lipoprotein (LDL)–receptor YWTD (amino acids 1373–1550). The arrow indicates the *ur41* mutation, Q550 → stop.

Table 1. The *nid-1* gene is required to position nerves dorsoventrally. Schematic drawings show the midlines as gray lines and axons as solid lines. Anterior is to the left. The *gfp* transgenes used to visualize the individual neurons are given in Methods.

	Genotypes			Genotypes	
	Wild type	<i>nid-1(-)</i>		Wild type	<i>nid-1(-)</i>
A. Wild-type DSL nerves (dorsal midline)	100%	9%	C. Wild-type anterior interneuron crossover (ventral midline)	95%	33%
Right DSL shifted to dorsal midline	0	21%	Multiple left-to-right crossovers	5%	67%
Left DSL shifted to dorsal midline	0	25%		$n = 89$	$n = 39$
Both DSL shifted to dorsal midline	0	45%	D. Wild-type DA and DB motor neurons (ventral midline)	96%	78%
	$n = 100$	$n = 100$	Longitudinal processes in left fascicle	4%	22%
B. Wild-type PVQ axon migrations (ventral midline)	100%	3%			
Left PVQ crossover	0%	77%	E. Wild-type DA and DB motor neurons (dorsal midline)	98%	61%
PVQ crossovers X2 or X3	0%	20%	Split dorsal nerve cord	2%	39%
	$n = 100$	$n = 100$		$n = 100$	$n = 100$

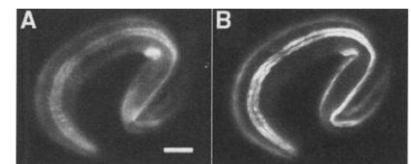


Fig. 4. Nidogen is associated with body wall basement membranes. **(A)** Larva stained to reveal anti-nidogen antibodies. Intense staining is associated with the basement membrane of the body wall muscle. **(B)** Muscle cells in the same larva visualized by using an anti-UNC-54 myosin monoclonal antibody. The muscle cells form four sublateral rows extending the length of the body. One muscle quadrant is in the plane of view. Scale bar, 10 μ m.

REPORTS

SDQR axon. This unexpected relationship suggests that nidogen has an effect on UNC-40-mediated signaling.

Our results show that nidogen affects the switch from circumferential to longitudinal

axon migration and that it helps determine where longitudinal nerves form along the dorsoventral axis. We propose that nidogen alters the SDQR axon response to guidance cues at the dorsal sublateral position. Nidogen or a

nidogen/laminin complex could act directly as a ligand for axonal guidance receptors, including UNC-40. This would be consistent with the recent description that extracellular matrix molecules can in vitro modify the behavior of growth cones in response to netrin-1 (27). It is also possible that nidogen creates a different basement membrane configuration that allows new interactions between the migrating axon and the basement membrane of the body wall muscle. To direct the switch from circumferential to longitudinal migration, nidogen may cause a weaker response to UNC-40-mediated circumferential guidance signals so that the axon can then be guided by longitudinal guidance cues. Alternatively, nidogen may be required for the axon to have a response to longitudinal guidance cues that is strong enough to overcome the effects of UNC-40-mediated signals at the dorsal sublateral position. At the dorsal and ventral midlines in the embryo, the nerve cords form along the edge of body wall muscle basement membranes and nidogen at this interface could influence midline crossing by affecting axon responses to midline guidance cues.

Table 2. The *unc-40* gene is epistatic to *nid-1* for SDQR axon positioning. Schematic drawings show the midlines as gray lines and axons as solid lines. Filled boxes represent basement membranes where nidogen is localized. Not shown are SDQR axons that joined other lateral longitudinal nerves. The SDQR cell body is sometimes positioned further ventrally in *unc-5*, *unc-6*, and *unc-40* mutants (22). Axon migrations were scored from cell bodies in either position. Anterior is to the left. The *unc-119::gfp* transgene was used to visualize the SDQR neurons. Alleles scored were *nid-1(ur41)* and *unc-40(e1430)*.

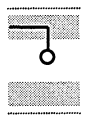
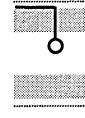
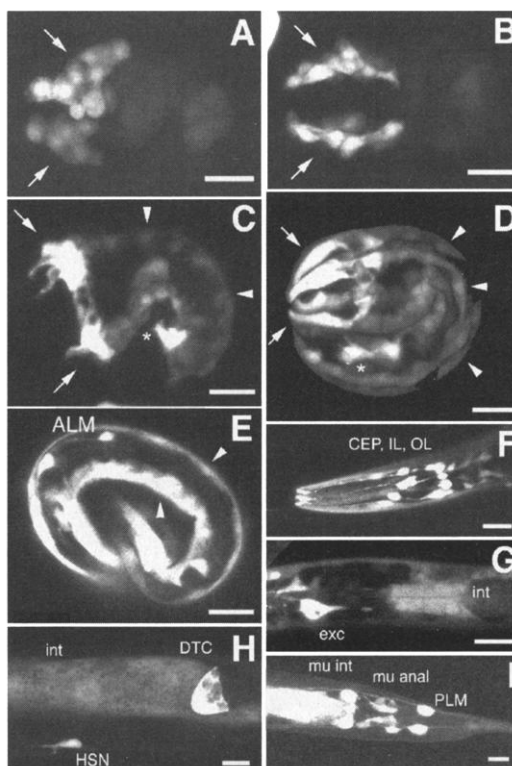
	Genotype			
	Wild type	<i>nid-1(-)</i>	<i>unc-40(-)</i>	<i>unc-40(-)</i> <i>nid-1(-)</i>
SDQR dorsal sublateral migration 	95%	42%	64%	65%
SDQR dorsal midline migration 	0	54%	0	0
SDQR ventral midline migration 	4%	0	21%	28%
	<i>n</i> = 100	<i>n</i> = 100	<i>n</i> = 100	<i>n</i> = 100

Fig. 5. Expression of the *nid-1* gene detected by using the *nid-1* promoter to drive GFP expression. Embryos (A, B, C, D, and E) and larvae (F, G, H, and I). (A and B) Shortly before (A) and at the beginning (B) of embryonic elongation, expression is detected in the Cep (cephalic), IL (inner labial) and OL (outer labial) neurons (arrows). (C, D, and E) During succeeding stages of elongation until hatching, expression is detected in body wall muscle (arrowheads), the intestinal and anal depressor muscle cells (*), and the ALM neurons. (F, G, H, and I) In the larva, expression is detected in the head Ceh, IL, and OL neurons (F), the excretory canal cell (exc) and anterior intestine (int) (G), the distal tip cells (DTC) and the HSN neurons (H), and posteriorly in the PLM neurons and the anal depressor and intestinal muscle cells (mu int and mu anal) (I).



References and Notes

1. M. Tessier-Lavigne and C. S. Goodman, *Science* **274**, 1123 (1996).
2. The *nid-1* allele was isolated by a clonal, F₂ screen using ethylmethanesulfonate as a mutagen. The starting strain, IM19 (*unc-119::GFP*), carries a transgene that expresses GFP throughout the nervous system (23). F₂ embryos were screened by epifluorescence microscopy for axon scaffold defects and by Nomarski microscopy for general morphological defects. The isolated mutant strains were back-crossed against wild-type (N2) five times to remove other possible mutations. The *ur41* mutation was mapped relative to *lon-3(e2175)* and *unc-76(e911)*. From the Lon non-Unc recombinants, 21 of 97 segregated *ur41*. Subsequently, *ur41* was mapped relative to *lin-25(n545)* and *unc-76(e911)*. One of six Lon non-Unc recombinants segregated *ur41*, which placed *nid-1* to right side of *lin-25*. By complementation test with chromosomal deficiencies, *arDf1* deleted *nid-1(ur41)* but not *odr-3*. These results ordered *ur41* between *lin-25* and *odr-3* of linkage group V, spanned by 28 genomic cosmids (*C. elegans* Genome Project). Pools of three to four cosmids were injected at 5 to 10 μg/ml per cosmid along with the dominant transformation marker, pRF4, which contains *rol-6(su1006)* (29) at 100 μg/ml into *ur41* animals carrying a dorsal sublateral nerve GFP marker transgene, *kyls123(zc21.2::GFP)* (30). The nerves were examined for the rescue of the *nid-1(ur41)* phenotype. Germ line transformation with one cosmid F54F3 (accession number Z79696) completely rescued the *ur41* phenotypes. An 11-kb PCR product that included the entire predicted coding sequence for the nidogen gene and 2.5 kb of 5' flanking sequence also rescued the phenotypes.
3. To analyze the migrations of different classes of neurons, we created strains by standard genetic crosses that contained GFP markers for different axons: *urIs13(unc-119::GFP)* for visualization of whole nervous system (23), *evIs82a(unc-129::GFP)* for visualization of DA and DB neurons (26) [for these and other cell names, see J. White, E. Southgate, J. Thompson, S. Brenner, *Philos. Trans. R. Soc. (London)* **B 314**, 1 (1986)], *rhlS4(glr-1::GFP)* for visualization of AVA, AVB, AVD, AVE, AVG, and PVC interneurons within the ventral nerve cord (31, 32), and *kyls39(sra-6::GFP)* for visualization of PVQ neurons (33). Images were obtained by using a Zeiss LSM 410 Invert Laser Scan

- microscope. For the electron microscopy analysis, animals were fixed with glutaraldehyde and osmium tetroxide (34). Five or six L4 or young adult animals were aligned within a small agar block, embedded, and sectioned together. Sections were poststained with uranyl acetate and lead citrate.
4. R. Durbin, thesis, University of Cambridge, Cambridge, England (1987).
 5. G. Garriga, C. Desai, H. R. Horvitz, *Development* **117**, 1071 (1993).
 6. S. Kim and W. G. Wadsworth, data not shown.
 7. The *nid-1(RNAi)* animals were generated as described previously [A. Fire *et al.*, *Nature* **391**, 806 (1998)] by using a 1-kb sequence from exon 8, which was cloned into pBluescript (Stratagene) as template for RNA synthesis. RNA was produced by both T3 and T7 RNA polymerase, and the reactions were pooled before being injected into the intestines of *eds20(unc-119::GFP)* transgenic animals. Phenotypes of the nervous system were observed under epifluorescence microscopy.
 8. Seven PCR fragments, including the whole coding sequence and intron region, were amplified from the genomic DNA of *nid-1(ur41)* animals. PCR fragments were cloned into a pBluescript vector and subsequently sequenced by automatic sequencer. The mutation was confirmed by sequencing two independent PCR fragments.
 9. U. Mayer, E. Kohfeldt, R. Timpl, *Ann. N.Y. Acad. Sci.* **857**, 130 (1998).
 10. J. W. Fox *et al.*, *EMBO J.* **10**, 3137 (1991).
 11. R. Timpl, J. C. Brown, *BioEssays* **18**, 123 (1996).
 12. F. D. Yelian, N. A. Edgeworth, L. J. Dong, A. E. Chung, D. R. Armant, *J. Cell Biol.* **121**, 923 (1993).
 13. R. F. Nicosia, E. Bonanno, M. Smith, P. Yurchenco, *Dev. Biol.* **164**, 197 (1994).
 14. P. Ekblom *et al.*, *Development* **120**, 2003 (1994).
 15. Y. Kadoya *et al.*, *Development* **124**, 683 (1997).
 16. Immunostaining was performed by using freeze-fragmentation and methanol-acetone fixation as previously described (35). Polyclonal antibodies raised against mouse nidogen and a mouse monoclonal antibody against myosin heavy chain B (UNC-54) were used. For costaining, anti-rabbit fluorescein-conjugated and anti-mouse rhodamine-conjugated secondary antibodies were used.
 17. Supplemental Web material is available at www.sciencemag.org/feature/data/1048303.shl
 18. T. Sasaki, W. Gohring, T. C. Pan, M. L. Chu, R. Timpl, *J. Mol. Biol.* **254**, 892 (1995).
 19. M. Hopf, W. Gohring, E. Kohfeldt, Y. Yamada, R. Timpl, *Eur. J. Biochem.* **259**, 917 (1999).
 20. D. G. Moerman, H. Hutter, G. P. Mullen, R. Schnabel, *Dev. Biol.* **173**, 228 (1996).
 21. P. L. Graham *et al.*, *J. Cell Biol.* **137**, 1171 (1997).
 22. S. Kim, X. C. Ren, E. Fox, W. G. Wadsworth, *Development* **126**, 3881 (1999).
 23. X. C. Ren, S. Kim, E. Fox, E. M. Hedgecock, W. G. Wadsworth, *J. Neurobiol.* **39**, 107 (1999).
 24. Transgenic strains were generated by standard methods (36). pIM#194, an expression construct for *nid-1*, was constructed by cloning the 2.5-kb 5' flanking region of *nid-1* into pPD 95.77 vector (from A. Fire). This GFP construct was coinjected at 10 μ g/ml with pRF4 at 100 μ g/ml. To establish a stable line, IM329 *urIs151* [pIM#194, pRF4], transgenes were integrated by γ -ray irradiation. For the ectopic expression construct of *nid-1*, constructs pIM#195, pIM#196, and pIM#197, were made by using the 7-kb genomic *nid-1* coding region, which was amplified by high-fidelity PCR, ligated to Nhe I-Bgl II-digested vectors, pPD96.41, pPD49.83, and pPD96.52 (from A. Fire). These vectors contained 5' flanking regulatory sequences of *mec-7*, *hsp16-41*, and *myo-3*, respectively (36). The *unc-119* regulatory sequence was amplified by using pIM175 as template (23), and cloned into the pPD49.26 vector (from A. Fire) to construct pIM#198. These constructs were injected at 10 μ g/ml, with pRF4 into *nid-1(ur41)*; *kyls123(zc21::GFP)* animals. The resulting strains are IM330 *urEx152* [pIM#195]; *nid-1(ur41)*; *kyls123(zc21::GFP)*; IM331 *urEx153* [pIM#196]; *nid-1(ur41)*; *kyls123(zc21::GFP)*; IM332 *urEx154* [pIM#197]; *nid-1(ur41)*; *kyls123(zc21::GFP)*; IM333 *urEx155* [pIM#198]; *nid-1(ur41)*; *kyls123(zc21::GFP)*. Ectopic expression of *nid-1* was checked by in situ hybridization. IM331 embryos collected 1 to 6 hours after being laid were heat-shocked at 29.5°C for 1 hour. After heat shock, embryos were placed at 20°C, grown to the L4 stage, and examined for mispositioned nerves. Of those treated, 96% ($n = 54$) of the animals had wild-type nerves. For IM330, IM332, and IM333 animals, 32% ($n = 41$), 53% ($n = 72$), and 97% ($n = 71$) have wild-type nerves. Detection of RNA in whole-mount *C. elegans* embryos was performed as described (37). AP-anti-Dig antibody was used for alkaline phosphatase (AP)-mediated detection. 4',6'-Diamidino-2-phenylindole (DAPI, 1 mg/ml) was included in the staining solution to allow nuclei to be identified by epifluorescence microscopy.
 25. S. Kim and W. G. Wadsworth, data not shown.
 26. A. Colavita, S. Krishna, H. Zheng, R. W. Padgett, J. G. Culotti, *Science* **281**, 706 (1998).
 27. V. H. Hopker, D. Shewan, M. Tessier-Lavigne, M. Poo, C. Holt, *Nature* **401**, 69 (1999).
 28. E. M. Hedgecock, J. G. Culotti, D. H. Hall, *Neuron* **4**, 61 (1990).
 29. J. M. Kramer, R. P. French, E. C. Park, J. J. Johnson, *Mol. Cell Biol.* **10**, 2081 (1990).
 30. C. M. Coburn and C. I. Bargmann, *Neuron* **17**, 695 (1996).
 31. A. C. Hart, S. Sims, J. M. Kaplan, *Nature* **378**, 82 (1995).
 32. A. V. Maricq, E. Peckol, M. Driscoll, C. I. Bargmann, *Nature* **378**, 78 (1995).
 33. E. R. Troemel, J. H. Chou, N. D. Dwyer, H. A. Colbert, C. I. Bargmann, *Cell* **83**, 207 (1995).
 34. J. Sulston, E. Schierenberg, J. White, J. Thomson, *Dev. Biol.* **100**, 64 (1983).
 35. W. G. Wadsworth, H. Bhatt, E. M. Hedgecock, *Neuron* **16**, 35 (1996).
 36. C. Mello and A. Fire, *Methods Cell Biol.* **48**, 451 (1995).
 37. G. Seydoux and A. Fire, *Methods Cell Biol.* **48**, 323 (1995).
 38. We thank C. Bargmann, J. Culotti, E. Hedgecock, H. Hutter, and D. Pilgrim for generously providing GFP marker strains, P. Yurchenco for providing the nidogen antibodies, D. Miller for providing the UNC-54 antibody, the *Caenorhabditis* Genetics Center for strains, A. Coulson for cosmids, M. Driscoll, G. Patterson, J. Schwarzbauer, and P. Yurchenco for comments on the manuscript, Z. Altun-Gultekin, C.-C. Huang, G. Kao, Y.-S. Lim, P. Yurchenco, and Q. Wang for helpful discussions, R. Patel for assistance with electron microscopy, and X.-C. Ren for superb technical assistance.

20 December 1999; accepted 15 February 2000

Receptors for Dopamine and Somatostatin: Formation of Hetero-Oligomers with Enhanced Functional Activity

Magalie Rocheville,¹ Daniela C. Lange,² Ujendra Kumar,¹ Shutish C. Patel,³ Ramesh C. Patel,² Yogesh C. Patel^{1*}

Somatostatin and dopamine are two major neurotransmitter systems that share a number of structural and functional characteristics. Somatostatin receptors and dopamine receptors are colocalized in neuronal subgroups, and somatostatin is involved in modulating dopamine-mediated control of motor activity. However, the molecular basis for such interaction between the two systems is unclear. Here, we show that dopamine receptor D2R and somatostatin receptor SSTR5 interact physically through hetero-oligomerization to create a novel receptor with enhanced functional activity. Our results provide evidence that receptors from different G protein (heterotrimeric guanine nucleotide binding protein)-coupled receptor families interact through oligomerization. Such direct intramembrane association defines a new level of molecular crosstalk between related G protein-coupled receptor subfamilies.

In the brain, somatostatin (SST) is found in interneurons as well as projection neurons in different regions, and is thought to be an important physiological regulator of numerous functions (1). The actions of SST are mediated by a family of G protein-coupled receptors (GPCRs) with five subtypes, SSTR1 to SSTR5, that are widely distributed with high concentra-

tions in the deeper cortical layers, the striatum, and most regions of the limbic system (2). Dopamine, like SST, acts through its own family of five GPCRs, D1R to D5R, that also display rich expression in the cerebral cortex, striatum, and limbic structures (3, 4). The SSTR and DR families share ~30% sequence homology and appear to be structurally related. Behavioral and clinical evidence indicates an interaction between the somatostatinergic and dopaminergic systems (5–8). Intracerebroventricular injections of SST produce dose-dependent neurobehavioral changes progressing from hyperkinesia to catatonia (6). The dual excitatory and inhibitory effects occur through differential activation of postsynaptic or presynaptic DRs, respectively (3). Central administration of dopamine likewise activates both SST and SSTRs

¹Fraser Laboratories, Departments of Medicine, Pharmacology, Therapeutics, Neurology, and Neurosurgery, McGill University and Royal Victoria Hospital, Montreal, Quebec H3A 1A1, Canada. ²Departments of Physics and Chemistry, Clarkson University, Potsdam, NY 13699, USA. ³VA Connecticut Healthcare System and New England Biomedical Research Center, Newington, CT 06111, USA.

*To whom correspondence should be addressed. E-mail: yogesh.patel@mcgill.ca